Insight into mechanics of AFM tip-based nanomachining: bending of cantilevers and machined grooves

R S J Al-Musawi[1,2], E B Brousseau[1], Y Geng[1,3], F M Borodich[1]

[1] *Cardiff School of Engineering, Cardiff University, Cardiff, United Kingdom*
[2] *Department of Mechanical Engineering, Kufa University, Iraq*
[3] *Centre for Precision Engineering, Harbin Institute of Technology, Harbin, People's Republic of China*

Email: BrousseauE@cf.ac.uk
raheem.almusawi@uokufa.edu.iq

Abstract. Atomic Force Microscope (AFM) tip-based nanomachining is currently the object of intense research investigations. Values of the load applied to the tip at the free end of the AFM cantilever probe used for nanomachining are always large enough to induce plastic deformation on the specimen surface contrary to the small load values used for the conventional contact mode AFM imaging. This study describes an important phenomenon specific for AFM nanomachining in the forward direction: under certain processing conditions, the deformed shape of the cantilever probe may change from a convex to a concave orientation. The phenomenon can principally change the depth and width of grooves machined, e.g. the grooves machined on a single crystal copper specimen may increase by 50% on average following such a change in the deformed shape of the cantilever. It is argued that this phenomenon can take place even when the AFM-based tool is operated in the so-called force-controlled mode. The study involves the refined theoretical analysis of cantilever probe bending, the analysis of experimental signals monitored during the backward and forward AFM tip-based machining and the inspection of the topography of produced grooves.

1. Introduction

We deal with theoretical and experimental studies of specific features of the AFM tip-based nanomachining. This type of nanomachining is based on the direct contact between the sharp tip of an AFM probe and the surface of a sample in order to induce material removal or modification at very small scales. The AFM tip-based nanomachining process, which is also referred to as AFM scratching or scribing, is currently the object of intense research investigations (see, e.g. reviews in [1-3]). Compared to other nanofabrication methods, which are essentially based on vacuum and mask-based processes [4-5], AFM tip-based nanomachining has a number of advantages. In particular, it generally requires less capital-intensive equipment, it is not restricted to the fabrication of planar features and it is not constrained to the processing of a limited set of materials [2,3,6].

It is known that the relative displacement of the tip over the material surface during the AFM scratching may be implemented along different processing directions (see, e.g. [7]); usually these are the backward and forward directions, which are illustrated in Figure 1a. It is obvious that the AFM cantilever working in the backward direction has always a convex deflection [7,8]. Let us consider the "forward direction". It is generally assumed (see, e.g. [9-12]) that during forward direction scratching, the bending of the cantilever is concave (see Figure 1b). However, from a theoretical point of view, there is no *a priori* reason to make this assumption. Indeed, the deformed shape of the cantilever during AFM tip-based nanomachining should depend on the particular loading conditions acting on the tip.

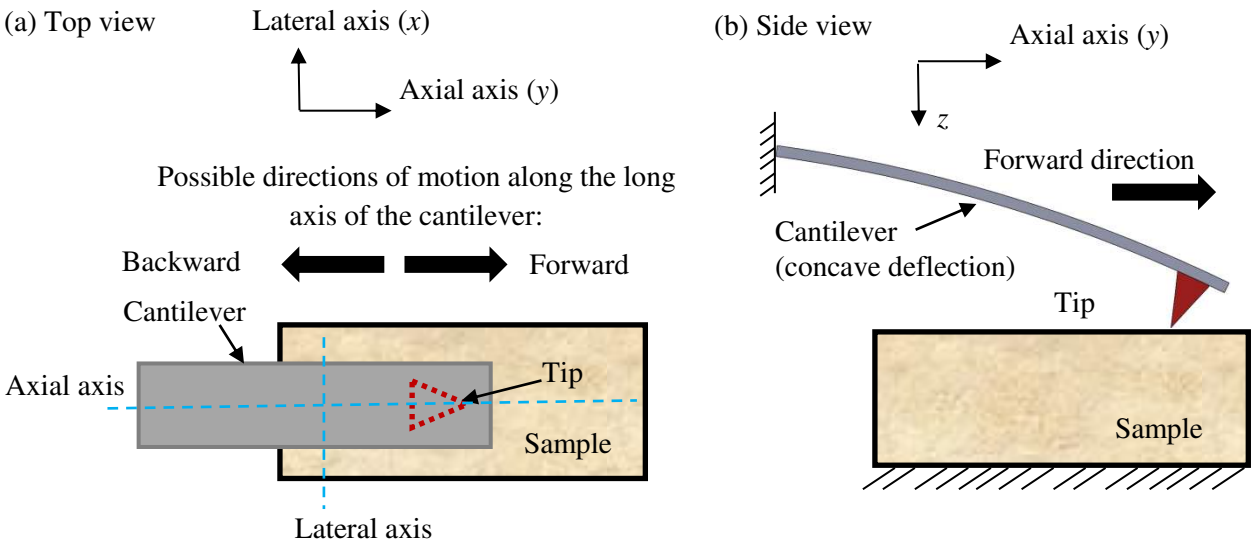

Figure 1. *The backward and forward AFM tip-based machining directions: (a) the top view perspective and (b) side view of the concave cantilever deflection.*

The paper is organised as follows. In Section 2, we present a theoretical analysis of the bending orientation of a cantilever that takes into account the specific tilt angle at which the probe is mounted within an AFM device. This analysis allows us to specify the actual directions of forces acting on the tip during a nanomachining operation. It is shown that under certain processing conditions, the deformed shape of the AFM cantilever probe working in the forward direction may change from a convex to a concave orientation. In Section 3, we describe the experimental methodology used in our studies including a description of the original AFM tip-based nanomachining set-up. We present the experimental cutting conditions used and explain the meaning of the cutting process steps reflected in the analysis of a typical output signal when monitoring the motions of the piezoelectric actuator on which the AFM probe is mounted. In Section 4, we present the experimental results when nanoscratching in different directions for varying loads. Note that one cannot observe directly whether the cantilever has convex or concave bending. Hence, one needs to interpret correctly the signals obtained. Because the deflected shape of the cantilever in backward and inclined backward directions is always convex, this can be used for the understanding of obtained signals. In turn, this knowledge is used to identify if concave bending is observed. It has been found that during actual AFM tip-based nanomachining tests in the forward direction, both convex and concave bending may be observed. The studies on a single crystal copper specimen have shown that the change of the cantilever bending from a convex to a concave shape may cause an increase of the depth and width of grooves machined up to 65% (in average about 50%), hence the change of the bending orientation affects drastically the depth and width of grooves machined.

2. Theoretical analysis of the deformed shape of the cantilever

The theoretical development reported in this section is based on the classic differential equation of the deflection curve of a beam [13]. The principal difference between the usual schemes for a tip-based nanomachining cantilever and the refined scheme of the present paper is that the inclination angle, α, between the cantilever and the surface of a sample is also considered in order to take into account the actual configuration of AFM systems. To the best of our knowledge, similar refined schemes were used only for lateral force analysis in the case of the frictional force AFM [14,15], while the aim of our analysis is to identify loading conditions on the tip during the AFM nanomachining process that determine the sign of the slope of the deflected cantilever at its free end.

A schematic illustration of the forces acting on the tip during nanomachining in the forward direction is given in Figure 2a and the corresponding free-body diagram is shown in Figure 2b. According to the literature for AFM machining, the y axis is directed along the beam and it is positive to the right; the z axis and the corresponding deflection w are positive downward; the bending moment is positive when it causes

compression in the upper part of the cantilever; and the curvature is positive when the cantilever is bent concave downward.

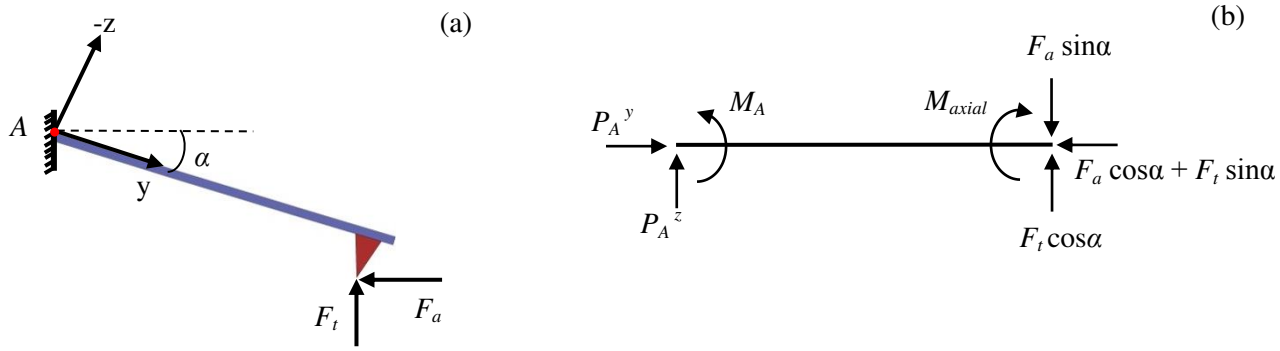

Figure 2. *(a) Schematic representation of the AFM probe during nanomachining in the forward direction and (b) corresponding free body diagram.*

Here F_t and F_a represent respectively the vertical and the horizontal forces acting at the pyramid tip, i.e. the force needed to keep the tip in the workpiece (the thrust), and the cutting force acting on the tip in the direction of cutting. These notations and terminology are adopted here to be consistent with notations used in the literature for conventional machining [16,17]. Because the forces F_t and F_a are shifted from the axis of the cantilever beam, they produce a moment at the free end of the cantilever M_{axial}, i.e. M_{axial} is generated by components of the forces of interaction between the probe pyramid tip and material of the sample. This is shown in the free body diagram (Figure 2b).

Due to the inclination angle, α, between the horizontal axis and the axis y of the cantilever, both F_t and F_a contribute to M_{axial} as follows:

$$M_{axial} = (h + t/2).F_a\cos\alpha + (h + t/2).F_t\sin\alpha \tag{1}$$

where h is the height of the tip and t is the thickness of the cantilever. Considering the equations of equilibrium, one can find the reaction moment M_A and reaction forces P_A^z and P_A^y at the built-in end of the cantilever

$$\begin{cases} P_A^y = F_a\cos\alpha + F_t\sin\alpha \\ P_A^z = F_a\sin\alpha - F_t\cos\alpha \\ M_A = M_{axial} + L(F_a\sin\alpha - F_t\cos\alpha) \end{cases} \tag{2}$$

where L is the length of the cantilever. Let us calculate now the bending moment, $M(y)$, at a distance, y, from the cantilever fixed end

$$M(y) = -M_A + yP_A^z. \tag{3}$$

Combining equations (1), (2) and (3), one gets

$$M(y) = -\left(h + \frac{t}{2}\right).F_a\cos\alpha - (h + t/2).F_t\sin\alpha + (y - L)(F_a\sin\alpha - F_t\cos\alpha) \tag{4}$$

The sign in the *differential equation* of the elastic (deformed) curve of the beam must be chosen to be consistent with the choice of coordinate directions and with the existing definition of positive bending [13,18] as that which produces curvature concave downward (hogging). Based on the coordinate directions used in Figure 2b and the fact that the angle of rotation of the cantilever, θ, is considered positive when clockwise with respect to the positive y axis, the basic differential equation of the deflection curve of the cantilever is expressed as

$$\frac{d^2w}{dy^2} = -\frac{M}{EI} \tag{5}$$

Its solution z = $w(y)$ defines the shape of the deflection curve. By combining equations (4) and (5), it follows:

$$EI\frac{d^2w}{dy^2} = (h + t/2)(F_a\cos\alpha + F_t\sin\alpha) + (L - y)(F_a\sin\alpha - F_t\cos\alpha) \quad (6)$$

Let us assume that the AFM probe is rectangular, and hence the flexural rigidity *EI* is fixed. This case represents the majority of probe designs. Then, the slope of the deflection curve may be found by integration of equation (6):

$$EI\frac{dw}{dy} = y(h + t/2)(F_a\cos\alpha + F_t\sin\alpha) + (F_a\sin\alpha - F_t\cos\alpha)(yL - y^2/2) + C \quad (7)$$

where *C* is a constant of integration. It follows from the boundary condition that the cantilever is built-in at the fixed end *A*, i.e. the slope is zero, that *C=0.* By substituting *y= L* in equation (7), one obtains the slope at the free end of the deformed cantilever

$$\frac{dw}{dy}(L) = \frac{L}{EI}[(h + t/2)(F_a\cos\alpha + F_t\sin\alpha) + (F_a\sin\alpha - F_t\cos\alpha)(L/2)] \quad (8)$$

Note that the thickness of the cantilever, *t*, is generally much smaller than its length, *L*, and the tip height, *h*. Hence, the above equation can also be simplified to:

$$\frac{dw}{dy}(L) = (L/EI)[h(F_a\cos\alpha + F_t\sin\alpha) + (F_a\sin\alpha - F_t\cos\alpha)/(L/2)] \quad (9)$$

Let us denote the moment generated at the fixed end of the probe by the force components acting on the tip and oriented in a direction perpendicular to the long axis of the cantilever as M_{normal}, i.e. $M_{normal} = L(F_t\cos\alpha - F_a\sin\alpha)$. Because $M_{axial} \approx h(F_a\cos\alpha + F_t\sin\alpha)$, one gets

$$\frac{dw}{dy}(L) = (L/EI)[M_{axial} - M_{normal}/2] \quad (10)$$

It follows from equation (10) and the sign convention of the slope of the deflected cantilever that

$$\begin{cases} \text{If } M_{axial} > (M_{normal}/2) \text{ then } \theta > 0; \text{ the cantilever shape at the tip end is concave} \\ \text{If } M_{axial} < (M_{normal}/2) \text{ then } \theta < 0; \text{ the cantilever shape at the tip end is convex} \end{cases} \quad (11)$$

One can see from equation (9) that in the general case the orientation of the deformed shape of the cantilever depends on three geometric parameters, namely, α, *h*, and *L* and two processing parameters, F_t and F_a. As a first approximation, it can be considered that the angle α is rather small, i.e. $\sin\alpha \approx 0$ and $\cos\alpha \approx 1$. Indeed, it is about 12° for actual AFM instruments. Putting $\sin\alpha = 0$ and $\cos\alpha = 1$, the equations (9) may be simplified further as

$$(EI/L)\frac{dw}{dy}(L) \cong hF_a - (L/2)F_t \quad (12)$$

Based on these coarse assumptions, it can generally be said that the bending of the cantilever during nanomachining in the forward direction is likely to be concave for increased values of axial cutting force, F_a, relatively to the thurst force, F_t.

Thus, it has been shown above that contrary to the assumption normally made in the AFM tip-based nanomachining literature, the deformed cantilever shape may be convex, especially for values of F_a that are small relatively to F_t. In the remainder of this paper, experiments are reported to verify whether both bending orientations can be observed in practice. Using both SEM micrographs of the grooves and AFM topography studies, it will be demonstrated further that this change of the convex to concave bending shape is accompanied by a drastic modification of the groove topography.

3. Experimental methodology

Let us describe the experimental methodology used in our studies including a description of the employed AFM instrument, the data acquisition system and the processing conditions implemented in the experiments. It is known (see, e.g. [19]) that most contemporary AFM devices are based on the use of the optical lever technique: a laser beam is focused on the free end of the AFM cantilever and the reflected beam is detected by a photodiode; it is also referred to as a Position Sensitive Photo Detector (PSPD). In practice, the PSPD of

an AFM instrument may consist of either two or four cells. The detection of vertical displacements of the reflected laser spot is obtained from the signal difference between the upper half and the lower half of the PSPD. This difference is commonly referred to as the "A-B" signal regardless of the number of cells. This is also the terminology adopted here. Thus, the difference in voltage output A-B gives a measure of the cantilever deflection. Here, we propose a new experimental set-up for determining the actual deflection of the cantilever during AFM nanomachining through monitoring and analysing the A-B and other voltages as explained in the next section.

3.1. Instrumentation

A commercial AFM instrument, the Park Systems XE-100, was employed. It was proposed to record three voltages in order to investigate the cantilever shape during AFM based nanomachining. These voltages are the following:

(i) the A-B signal that corresponds to the vertical motion of the free end of the cantilever,
(ii) the Y scanner signal that corresponds to the lateral stage motion of the X-Y stage, and
(iii) the monitoring of the Z-detector signal that provides information about the vertical motion of the cantilever at its built-in end.

To clarify the meaning of the above signal outputs, we describe their physical interpretation: (i) variations of the A-B signal detected by the PSPD is used by the feedback loop of the AFM instrument to monitor the vertical deflection of the free end of the cantilever; (ii) variations of the Z-detector signal (it is provided by a strain gauge sensor mounted on the piezo-electric actuator, referred to as Z scanner in Figure 3) is also an essential part of the AFM feedback loop as the Z scanner drives the vertical displacement of the probe at its fixed end; and (iii) monitoring of variations of the Y stage signal (sent by the AFM controller to a lateral piezo-electric actuator, which is used to drive the in-plane motions of the AFM stage) enables the accurate time determination of the beginning and end of the nanomachining operations realised in this study.

A data acquisition (DAQ) set-up was utilised to capture these three specific output signals during the nanomachining operations. This setup includes a Signal Access Module (SAM) from Park Systems, the NI 9223 module from National Instrument, and the LabVIEW software connected to the SAM. A schematic description of the AFM set-up utilised for tip-based nanomachining is shown in Figure 3.

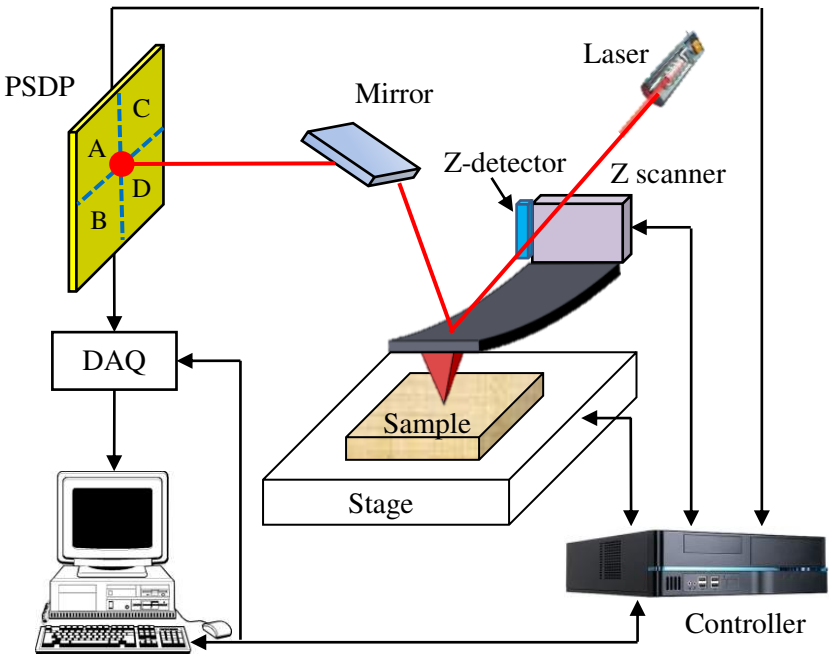

Figure 3. *Schematic description of the AFM tip-based nanomachining set-up.*

The majority of the experiments were performed on a single crystal copper sample. The probe used for conducting the machining operations on the copper sample was the DNISP type from Bruker. Such a probe

is typically utilised for nanoindentation and nanoscratching tests since it is designed with a relatively high spring constant. This probe had a rectangular cantilever made of stainless steel while its tip was a 3-sided diamond pyramid formed by 3 right angle planes. The tip apex may be reasonably approximated by a sphere. In this way, it was determined to have a radius of 70 nm using Scanning Electron Microscopy (SEM) imaging.

Another specimen made of polycarbonate (PC) was also employed to confirm the results observed with the copper workpiece. For the PC specimen, the nanomachining operations were conducted with a different probe - the TESPD type from Bruker. The TESPD type is coated with a diamond-like carbon layer for increased tip lifetime. The particular TESPD probe utilised had a nominal tip radius of 15 nm.

The accurate knowledge of the interaction force between the tip and sample requires the calibration of both the optical lever sensitivity and spring constant of the cantilever. Thus, the spring constant of the TESPD probe was determined using the Sader method [20] and found to be 56 N/m, while, for the DNISP probe, it was provided by manufacture and given as 221 N/m. The calibration of the normal sensitivity was done through fitting the slope of the force-distance curve, which is obtained by pressing the probe tips against a hard surface (fused silica in our case).

After completion of the machining process, another AFM probe, namely the CSG model from NT-MDT, was utilised for the purpose of recording the topography of the obtained grooves.

3.2. Experimental cutting conditions

The machining tests were conducted along different orientations, namely in the forward and backward directions as well as at inclined angles with respect to the main axis of the cantilever, as illustrated in Figure 4.

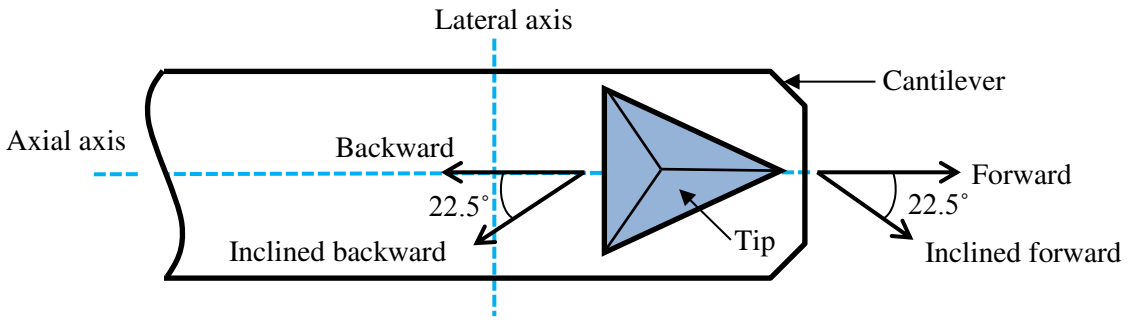

Figure 4. *Considered cutting directions with respect to the cantilever orientation and tip geometry.*

For each direction, several tests were carried out and between each of them, the normal force set by the user was gradually increased. In this way, the range of applied normal loads was comprised between 13 μN and 39 μN and 3.1 μN and 4.4 μN for the Cu and PC sample, respectively. The cutting parameters that were adopted during the experimental trials are summarised in Tables 1 and 2.

Table 1. *Machining conditions for the copper sample*

Probe type		DNISP
Groove length (μm)		15
Machining speed (μm/s)		5
Set normal force (μN)	Forward direction	20, 23, 24, 26, 27, 30, 31, 34, 36, 39
	Backward direction	13, 20, 27, 34

Table 2. *Machining conditions for the PC sample*

Probe type		TESPD
Groove length (µm)		15
Machining speed (µm/s)		3
Set normal force (µN)	Inclined forward (22.5°)	3.1, 3.4, 3.8, 4.1, 4.4
	Inclined backward (22.5°)	3.1, 3.4, 3.8, 4.1, 4.4

The cutting speed along the length of a processed groove was kept constant for all experiments at 5 µm/s and 3 µm/s for the Cu and PC specimen, respectively. Machined grooves were separated by a distance of approximately 20 µm to avoid any influence of a previous cut on the current groove being machined, such as the presence of material pile-ups or residual stress. SEM inspections were used for the qualitative observation of the grooves, while quantitative measurements (i.e. the depth and width of the grooves) were conducted on the same AFM instrument using CSG probes in contact mode. All experiments were conducted in a temperature-controlled laboratory, which was set at 21 ˚C ± 0.5 ˚C.

3.3. Analysis of the Z-detector output signal

Let us analyse in detail a typical Z-detector output signal (Figure 5). The signal was recorded during cutting of a groove in the PC sample along the backward direction. As noted in Figure 5, it is divided into five consecutive steps, which correspond to the regions “A”, “B”, “C”, “D” and “E”. The physical interpretation of each of them is given below.

First step (region A): This step takes place after the initial approach of the tip onto the surface of a specimen. In this case, the tip is in static contact with the sample but the applied normal force is very low. More specifically, it is typically in a range between a few nN to a few tens of nN as defined by the AFM user. Based on the knowledge of the normal spring constant of the probe and the sensitivity of the PSPD, this load corresponds to a given A-B output voltage, V_0, as illustrated with Figure 6.

Second step (region B): Between point 1 and point 2 in Figure 5, the normal load is increased to another user-defined value, which is sufficiently high to induce plastic deformation. In this example, it was set at 3.4 µN. During this step, the tip penetrates into the processed material as the probe is moved down vertically towards the sample due to the extension of the Z scanner. During this step there is no lateral motion of the AFM. Therefore, this step also corresponds to the loading cycle of a nano indentation process. The vertical motion of the probe stops when the A-B signal of the PSPD reaches a new value, which is illustrated as V_1 in Figure 6. As seen in the plot of Figure 5, the Z-detector signal increases sharply between point 1 and point 2. Thus, for the remainder of this paper, it is important to note that, when the Z scanner extends, and consequently the probe moves towards the sample surface, the Z-detector voltage increases. On the contrary, when the probe moves away from the sample, as a result of the contraction of the Z scanner, this signal decreases.

Third step (region C): This may be referred to as a transition step. In particular, at point 2 in Figure 5, the motion between the sample and the probe starts. Thus, an axial cutting force, F_a, is now also applied on the tip in addition to the thrust force, F_t. As presented in Section 2, the resulting change in the moment M_{axial} on the free end of the cantilever also modifies its deflection angle, θ. Consequently, the generation of F_a also modifies the A-B signal on the PSPD as a result of the optical lever principle. For this reason, the vertical position of the probe is automatically adjusted through the feedback loop of the AFM system. In this example, contraction of the Z scanner takes place to raise the probe until the A-B output reaches a target value, which corresponds to the voltage attained prior to the start of the lateral motion of the step. Thus, this voltage value also corresponds to V_1 as referenced in Figure 6. During this transition step, the Z-detector signal output varies until a steady-state configuration is reached, which is illustrated with point 3 in Figure 5.

Fourth step (region D): The time elapsed between points 3 and 4 corresponds to the actual machining of a groove as a result of the relative motion between the AFM tip and the surface of the sample along a pre-defined path.

Fifth step (region E): This step is reached when the lateral motion is stopped. The AFM tip contacts the bottom of the groove, however, the applied normal load reduces rapidly to the small value defined for the approach process (the first step).

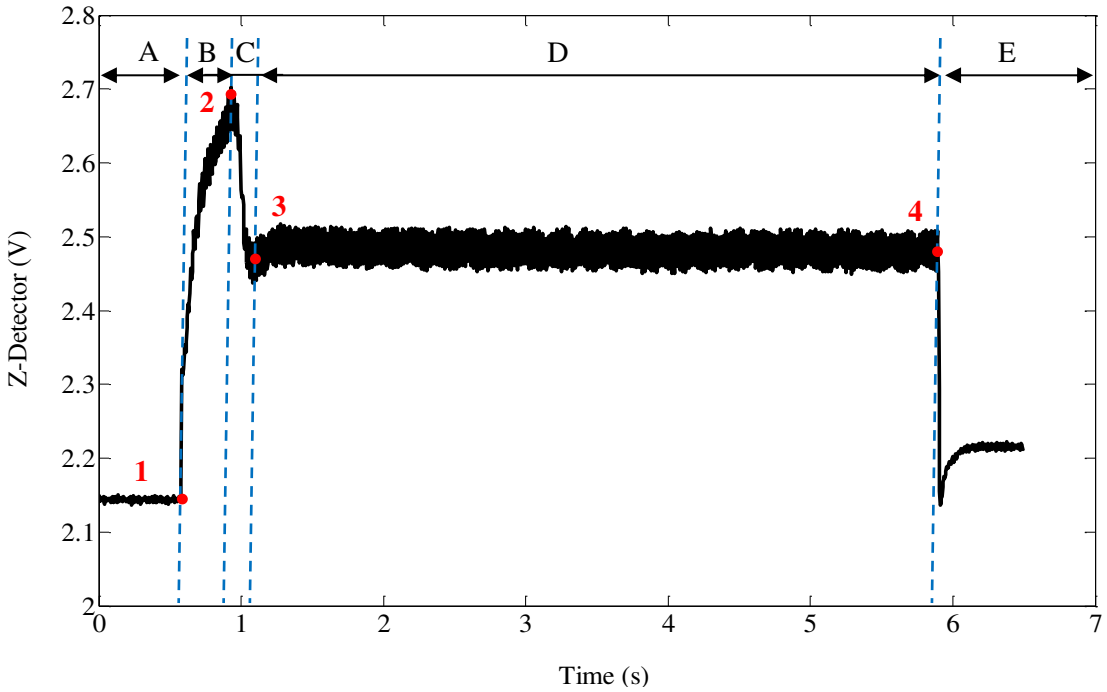

Figure 5. *Example of Z-detector signal recorded in the backward direction. In this example, the data were acquired when machining the PC sample with a set normal load of 3.4 μN.*

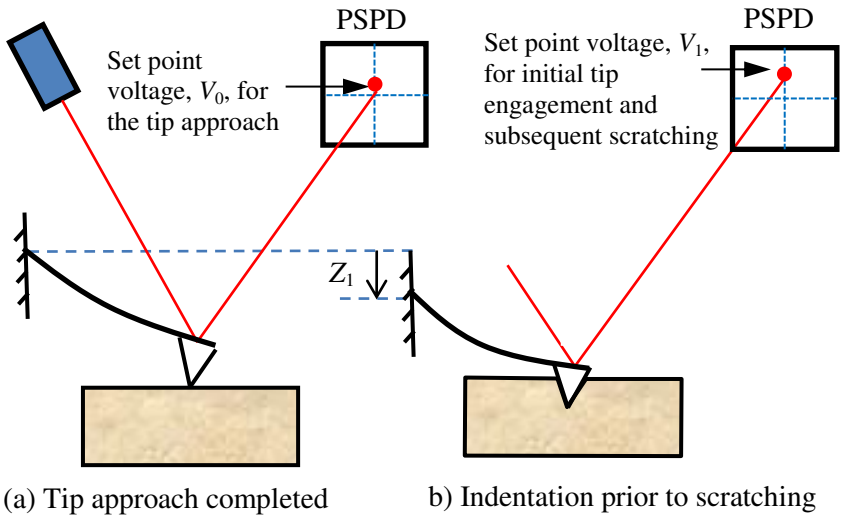

Figure 6. *A sketch of the probe and the PSPD status corresponding to: (a) the approach process (the first step) and (b) the initial tip penetration into the specimen (the second step).*

The observations reported in this paper rely significantly on the interpretation of the Z-detector output. Hence, the introduction of the above steps of a typical signal is given to avoid misunderstandings of the signal analysis. Figure 6 demonstrate the statuses of the AFM probe and the PSPD that correspond to the first step (the approach process) and the second step (the tip penetrates into the processed material sample).

4. Experimental studies of nanomachining with different process directions

Here we present the experimental results on nanomachining in the different directions for varying loads. Because one cannot observe directly whether the cantilever has convex or concave bending, one needs to interpret correctly the signals obtained. Because the deflected shape of the cantilever in backward and inclined backward directions is always convex, first, the Z-detector and PSPD (A-B) voltage signals in these directions are monitored and analysed. This analysis is performed mainly to help with an understanding of the physical meaning of these signals. Then, the knowledge about AFM outputs voltages gained is used to identify if concave bending is taking place during nanomachining in the forward direction. It is shown that during actual AFM tip-based nanomachining tests in the forward direction, both convex and concave bending are observed in the experiments.

4.1. Nanomachining with backward and inclined backward directions

Let us present several illustrative examples of data collected during machining of two material samples at varying loads. Figure 7 shows a selection of the Z-detector output signals for these samples. The signals in Figure 7a and Figure 7b were collected during machining of the Cu sample along the backward direction respectively with normal loads of 13 μN and 34 μN. The signals in Figure 7c and Figure 7d were collected during machining of the PC sample along the inclined backward direction respectively with normal loads of 3.1 μN and 4.4 μN. These four plots correspond to the Z-detector output voltage signals obtained for the smallest and the highest values of the normal loads for each material.

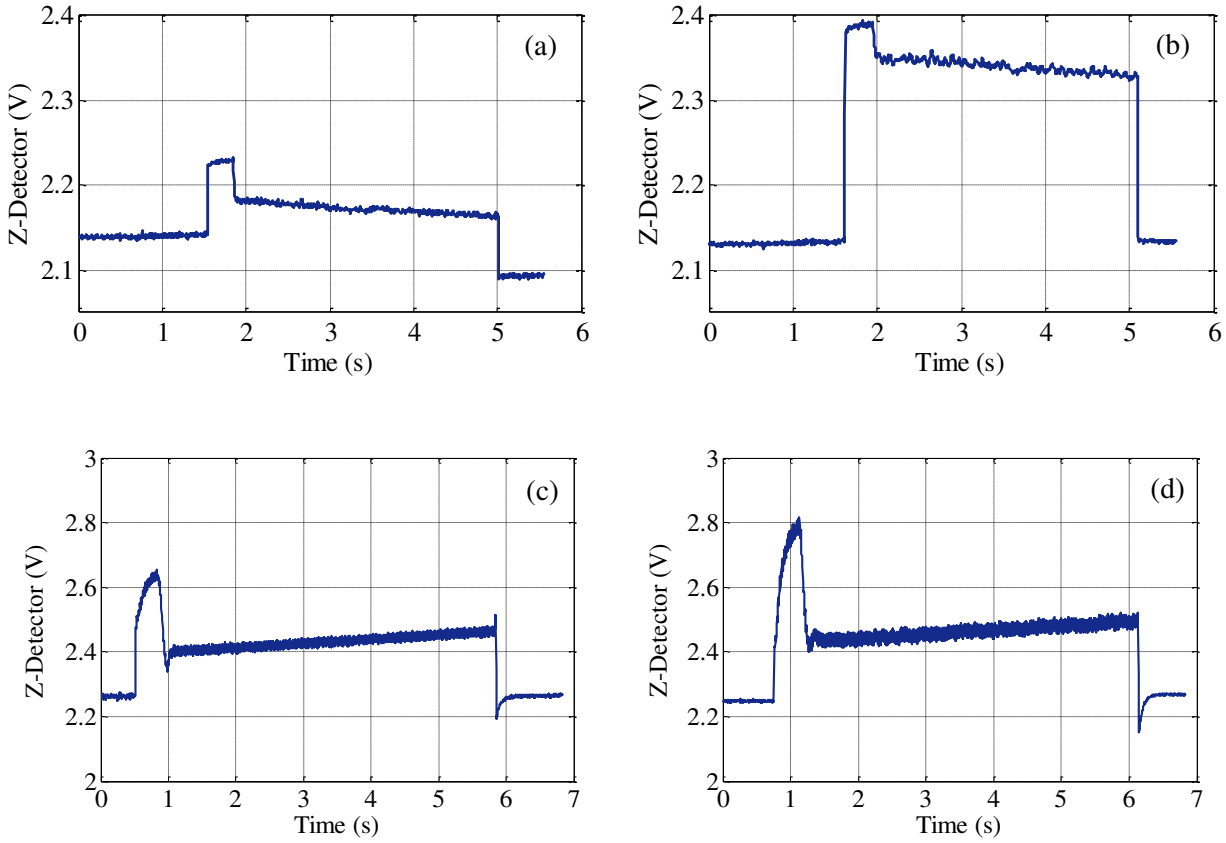

Figure 7. *The Z-detector output signals recorded during processing of the material samples: the Cu sample machined along the backward direction with normal loads of (a) 13 μN and (b) 34 μN and the PC sample machined along the inclined backward direction with normal loads of (c) 3.1 μN and (d) 4.4 μN respectively.*

Figure 8 displays an example of a typical A-B voltage signal recorded when processing along these directions. The monitored Y stage signal is also superimposed in this figure in order to associate the

fluctuation of the A-B voltage at the start and the end of the lateral motion of the AFM stage. From the magnification shown with Figure 8, it is observed that the A-B signal increases as soon as the motion of the Y stage begins. As it has been discussed in section 3, this increase is the result of the change in the deflection angle of the cantilever at its free end following the generation of the axial force, F_a, on the tip. In particular, for the backward and inclined backward machining configurations, the direction of F_a is always pointing away from the fixed end of the probe. Consequently, the deflection angle of the cantilever increases upon the start of the stage motion.

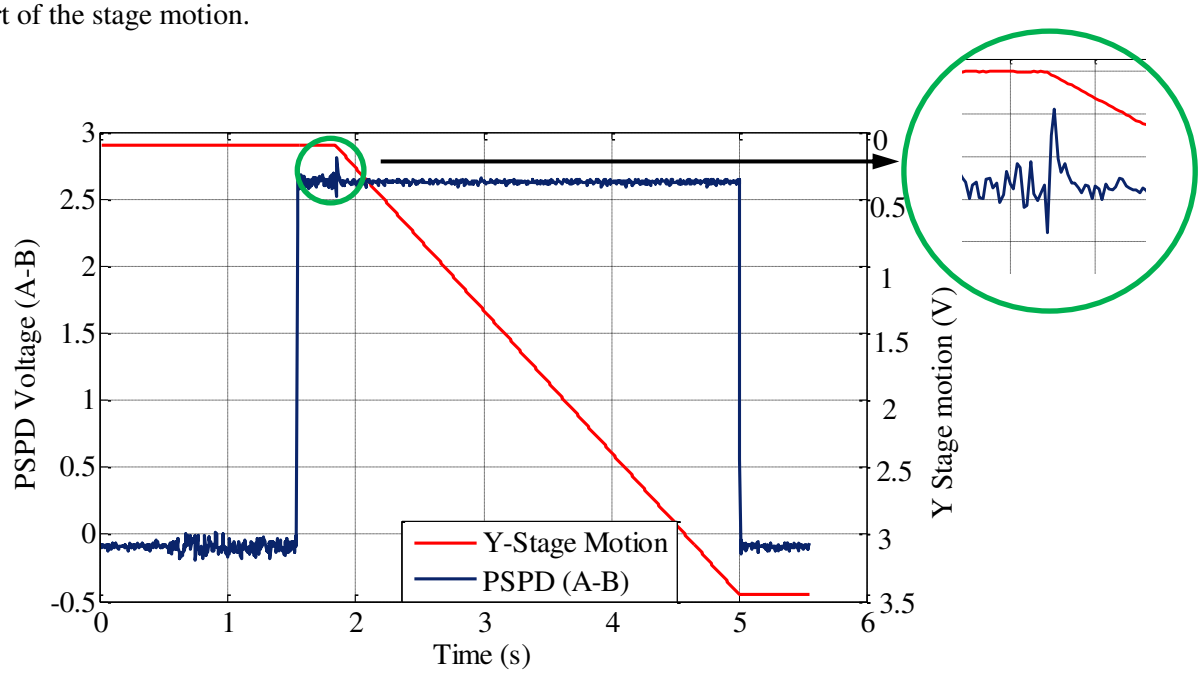

Figure 8. *Typical voltage signals corresponding to the vertical (A-B) and Y axis motions recorded during processing in the backward and inclined backward directions. The inset plot shows the change in the A-B voltage as soon as the lateral motion of the stage starts.*

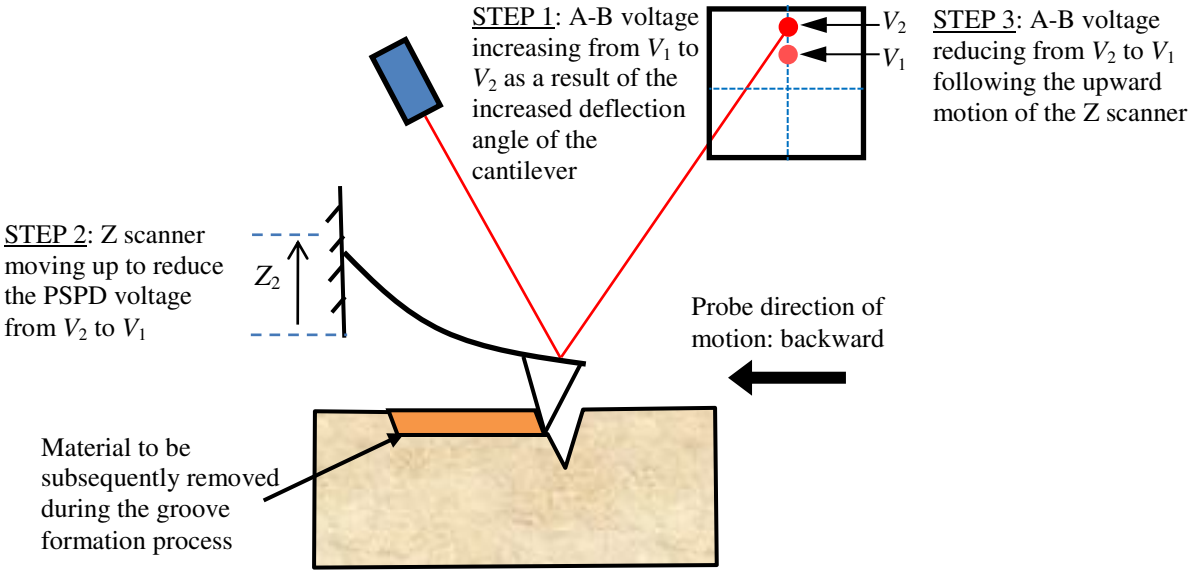

Figure 9. *Illustration of the sequence of events leading to the observed output signals upon initiation of the Y stage motion for backward and inclined backward machining:*

As observed in Figure 8, and as explained in Figure 9, the increase of the deflection angle leads also to the increase of the A-B signal on the PSDP. As all the experimental plots in Figure 7 show, the Z scanner raises

the probe to return the A-B voltage to its set value. This can indeed be observed as the Z-detector signal decreases in all cases during the time interval referred to as "region C" in the previous section.

Thus, the resulting shape of the deformed cantilever stays convex throughout machining in the backward and inclined backward directions due to the fact that F_a is pointing away from the fixed end of the cantilever along these cutting directions.

4.2. Shape of the deflected cantilever during nanomachining in the forward direction

Profiles of the Z-detector voltage corresponding to machining in the forward direction are reported and compared with these obtained in the backward direction. The results presented in this section are those obtained when processing the Cu sample in a pure forward direction. Depending on the load applied, three different types of voltage profiles may be observed corresponding to the quasi-static behaviour of the cantilever. These three types are associated with normal loads that are 1) relatively low (between 20 µN and 23 µN), 2) intermediate (between 24 µN and 27 µN) and 3) high (between 31 µN and 39 µN).

4.2.1 The deflection of the cantilever at low loads

As the above theoretical analysis shows, it would be reasonable to expect that in the pure forward direction machining, the A-B voltage of the PSPD drop as soon as the motion of the Y stage begins. Indeed, the axial force F_a is pointing towards the fixed end of the probe in this case. As a result of this orientation, the deflection angle of the cantilever should decrease once the displacement of the stage is initiated. Consequently, it would also be expected that, the probe should be lowered towards the sample by the Z scanner in order to raise the PSPD voltage back to its set value. If this downward vertical motion of the probe takes place, then an increase in the Z-detector signal should be recorded with the data acquisition system. However, the opposite result was observed when processing with low normal loads.

Let us present an illustrative example of data collected during machining of the Cu sample in this range of loads. Figure 10 shows the Y stage output signal and Z-detector output signal captured during machining along the pure forward direction for the applied load 20 µN. From this figure, it is observed that the profile of the Z-detector signal is similar to these obtained in the backward direction.

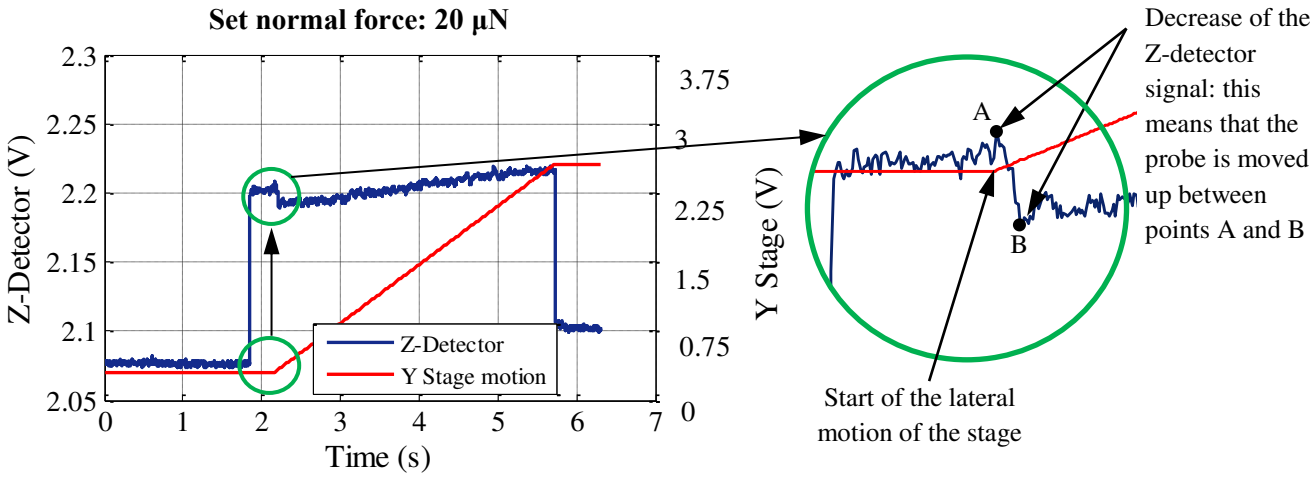

Figure 10. *Recorded Z-detector and Y stage output signals when processing the Cu sample along the forward direction for a set normal load of 20 µN. Note that for the inset higher magnification image, the Y stage signal was deliberately shifted up for clarity purpose.*

In particular, it can be seen with the magnified image in Figure 10 that the Z-detector decreases once the motion of the Y stage begins. This means that the probe was raised. A possible reason for such behaviour is that the initial stage displacement results in a sliding motion of the tip along the face of the indent formed during the previous time interval when the AFM stage was still static. This sliding motion results in the PSPD voltage to increase, as illustrated in Figure 11. Consequently, the Z scanner raises the probe until the PSPD voltage reduces back to its set value. Therefore, based on the fact that the probe is moved up at the

start of the groove and that the overall profile of the Z-detector signal is similar to that obtained in the backward direction, it is concluded that the deformed shape of the cantilever is convex during the machining process for this lower range of set normal forces. Thus, the value of the force F_a was too small to change the cantilever shape (see equation (12)).

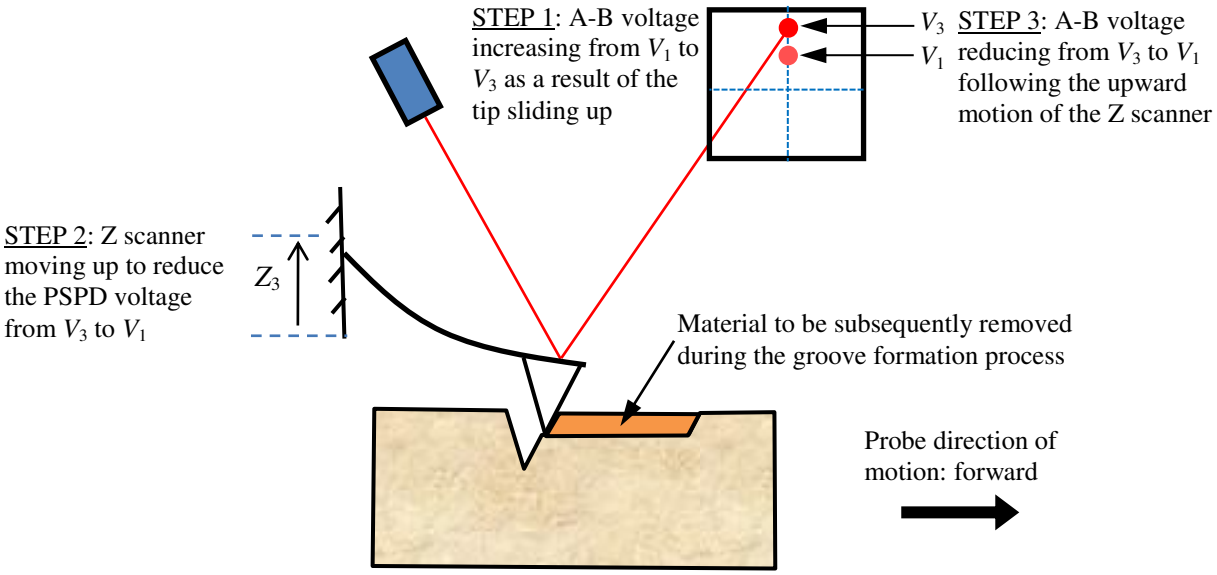

Figure 11. *Illustration of the tip sliding up the face of the initial indent and the subsequent series of events with respect to the A-B voltage variation on the PSPD and the associated response of the Z scanner via the force-controlled feedback loop.*

4.2.2 The deflection of the cantilever at medium loads

In this range of loads, one can observe the different behaviour of the profiles of the Z-detector output voltage in comparison with the behaviour of these profiles recorded in the backward direction. The signals in Figure 12 were captured during machining along the pure forward direction for an applied load 24 μN.

It can be seen from this figure that the probe is brought down towards the sample as soon as the Y stage initiates its displacement. This is the opposite motion to that reported earlier in section 4.2.1 when conducting experiments with smaller loads. Indeed, the lowering of the probe via the feedback loop of the AFM at this particular stage of the process is realised in response to a reduction in the deflection angle at the free end of the cantilever. This decrease in the deflection angle at the start of the displacement of the stage is a consequence of the generated axial force, F_a, being induced on the tip while the tip is also sticking on the initial indent (as opposed to sliding along it).

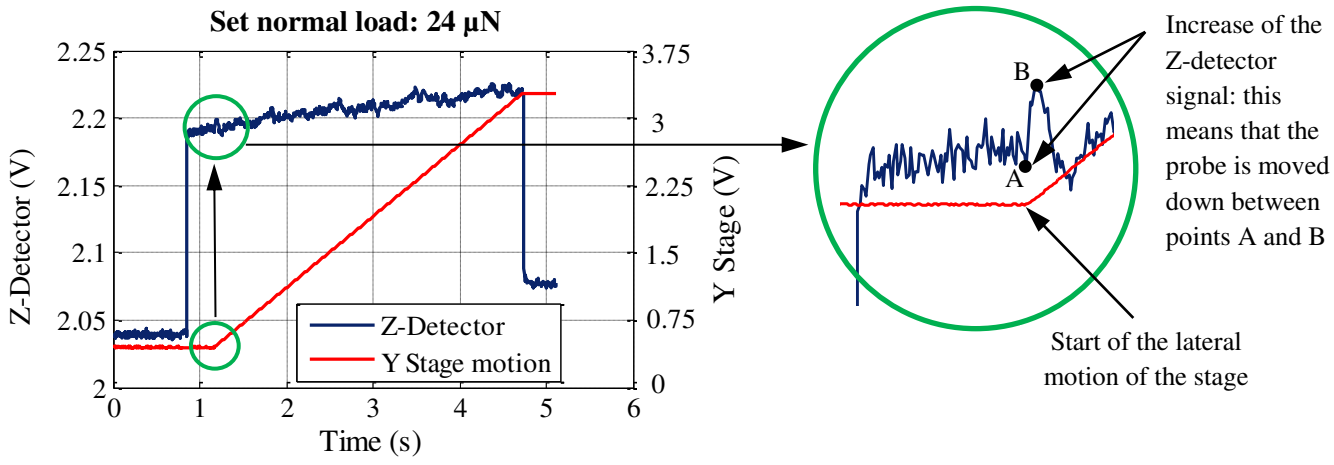

Figure 12. *Recorded Z-detector and Y stage output signals when processing the Cu sample along the forward direction for a set normal load of 24 μN.*

The sequence of events leading to the observed output signals upon initiation of the stage motion is illustrated with Figure 13. It should be noted that this observation could also be made when processing with a set normal load of 26 µN.

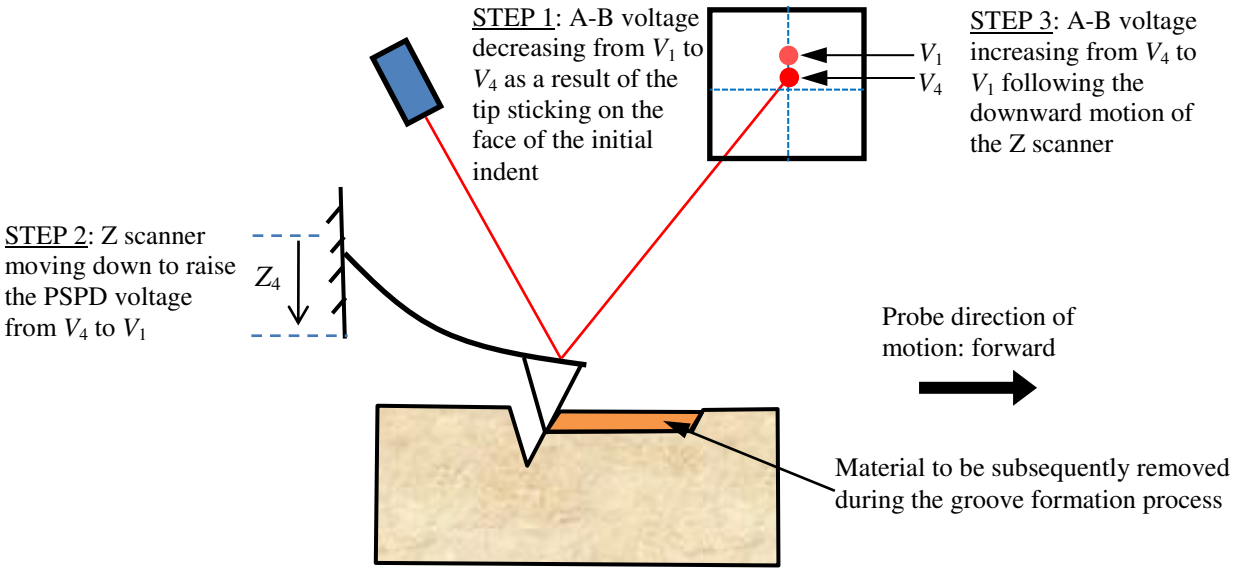

Figure 13. *Illustration of the probe being lowered upon the start of the lateral motion of the stage as a result of the tip sticking on the initial indent.*

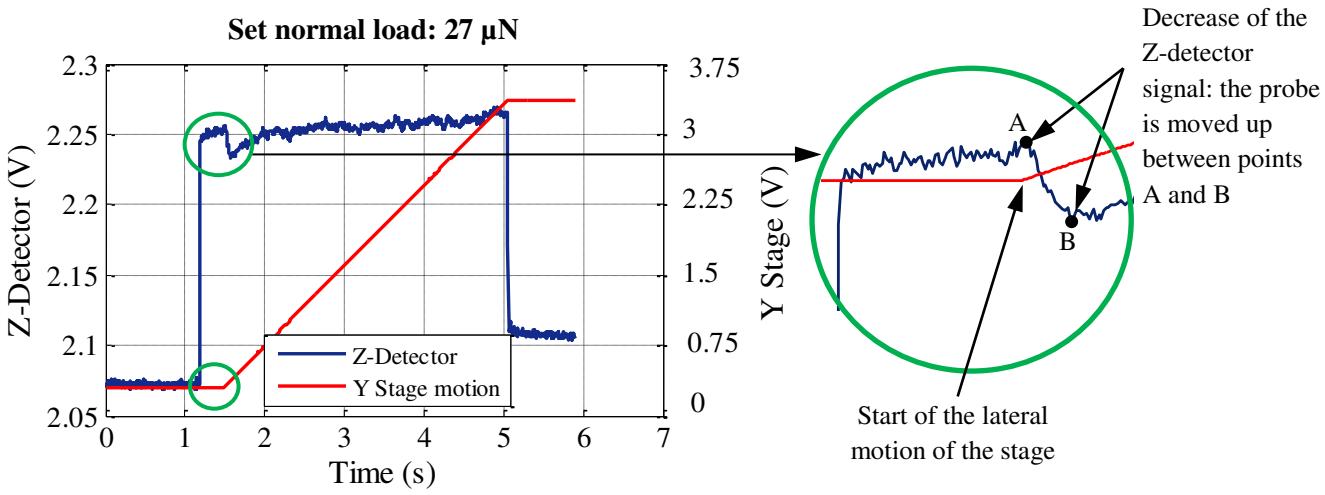

Figure 14. *Recorded Z-detector and Y stage output signals when processing the Cu sample along the forward direction for a set normal load of 27 µN.*

However, for 27 µN, it is the sliding motion of the tip, which was found to govern the response of the Z scanner motion upon the initiation of the lateral displacement of the stage (see Figure 14). Thus, it can be said that, in this intermediate range of set normal loads, a mix between tip sliding and tip sticking phenomena was obtained when initiating the machining operations. In addition, the cantilever shape also stayed convex during machining in this range of medium loads. Thus, the generated axial force F_a was not enough to change the cantilever deflected shape.

4.2.3 The deflection of the cantilever at high loads

In this third and highest range of set normal forces, the recorded data showed that the tip sticking effect consistently dominated the behaviour of the AFM probe during the initial motion of the stage. Most importantly, however, a significant phenomenon was observed during the subsequent groove machining process. This is illustrated by Figure 15 in the case of a set normal load of 31 µN. In particular, it can be seen from this figure that the Z-detector signal increases significantly about half-way through the cutting of the

groove. This rapid and high increase in the Z-detector signal compared with these reported earlier with low and medium loads shows that the feedback loop of the AFM suddenly drove the probe down as the groove was being cut. This was realised to ensure the A-B voltage output of the PSPD was maintained to a set target value. At the same time point, the PSPD voltage also started displaying more pronounced oscillations around this target value.

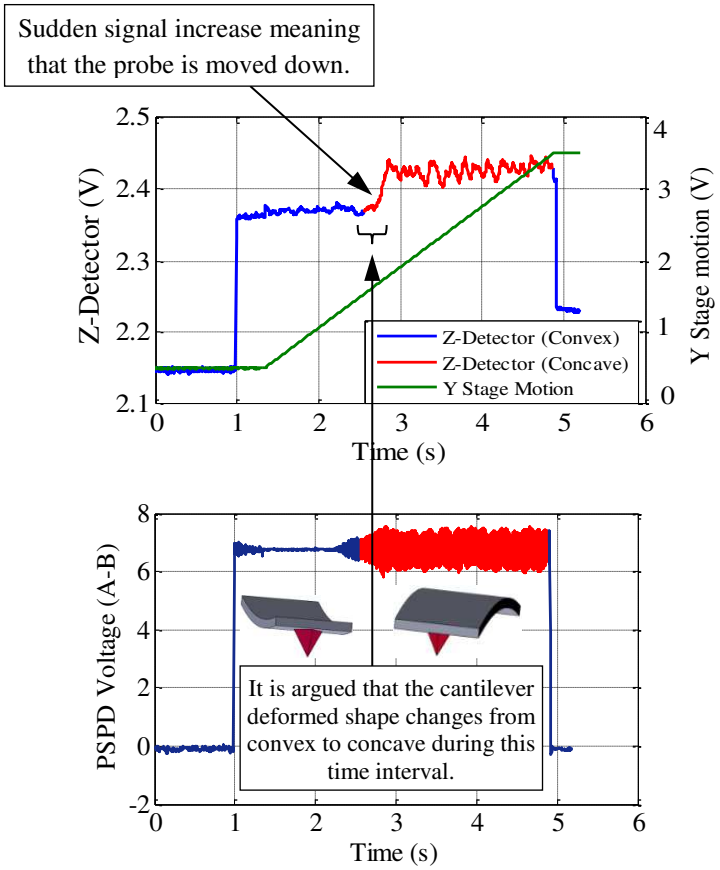

Figure 15. *The recorded signals with the normal load of 31 μN during processing the Cu sample along the forward direction: (a) the Z-detector (the sudden signal increase means that the probe is moved down); and (b) the (A-B) PSPD voltage output signals. The blue and red lines correspond respectively to the convex and concave deflections of the cantilever.*

The hypothesis put forward to explain such observation during this particular short time interval is that the bending of the cantilever at its free end changes from a convex orientation to a concave one. To support this hypothesis, it is argued that the axial force, F_a, acting on the tip is gradually increasing along the length of a machined groove. Further investigations are required to elucidate in a comprehensive manner the reason behind this increase in F_a during the groove formation process itself. The hypothesis that may be put forward at this stage to explain such a change in the cutting force is that it could be the result of the combined effect of 1) the accumulation of piled-up material in front of the tip and 2) the strain hardening of the material ahead of the tip. In particular, the gradual accumulation of pile-up on the tip rake face augments the contact area between the tip and the material, which in turn, raises the force acting of the tip. Strain hardening of the material may also be considered as a possible effect. Indeed, when increasing the value of the set normal load, the resulting larger volume of material subjected to plastic deformation around the tip may also be expected to be associated with an augmentation of the dislocations density in this region. Consequently, when the tip moves across the surface of the sample, it can also be reasonably expected that the occurrence of dislocation entanglements should increase and thus, that the number of movable dislocations should reduce. Regardless of the specific physical phenomon at play, an increase in F_a results in a reduction of the deflection angle at the free end of the cantilever, which may eventually become negative and lead to the feedback loop observed reaction, as illustrated with Figure 16.

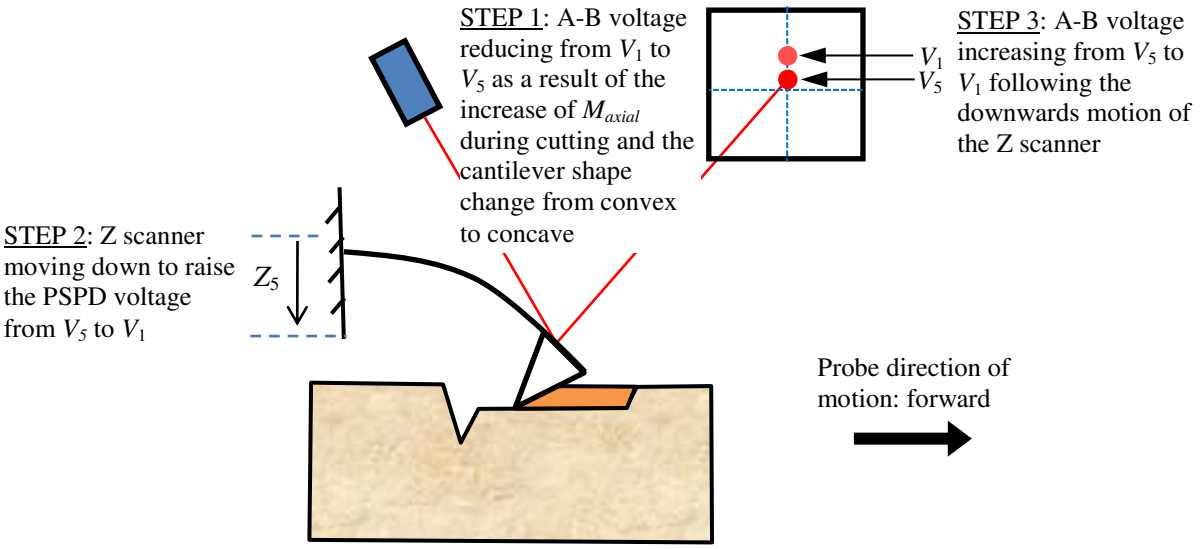

Figure 16. *Illustration of the bending orientation of the cantilever changing from convex to concave during the machining of a groove and the associated Z scanner response.*

Based on the analysis of other recorded Z-detector signals, it can be reported that such transition from convex to concave bending during the actual groove formation process could also be observed when machining with all the other considered loads in this range. For example, Figure 17 displays the signals obtained for the highest load tested, which was 39 µN. The main comment that can be added when analysing this figure is that the occurrence of the change in the bending of the cantilever occurs sooner along the groove in this case.

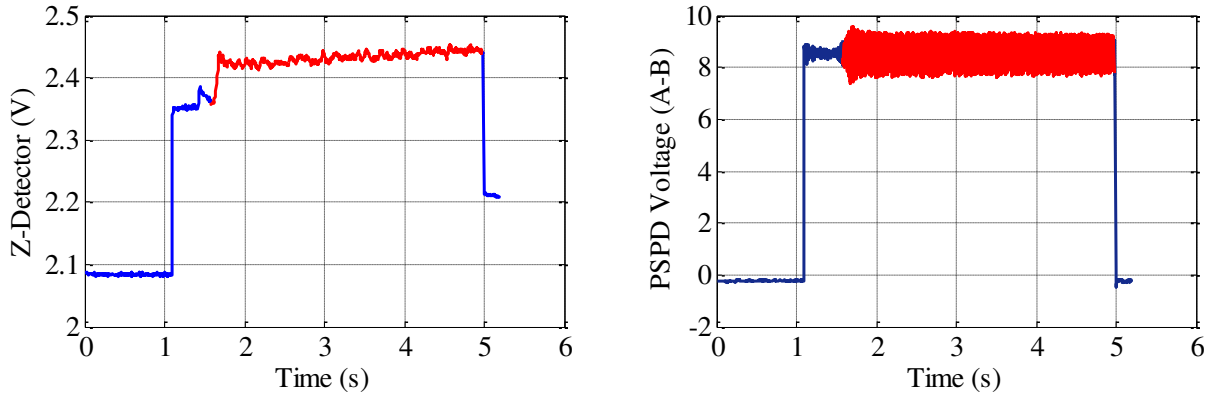

Figure 17. *The recorded signals with the normal load of 39 µN: (a) Z-detector and (b) A-B signals. The blue and red lines correspond respectively to the convex and concave deflections of the cantilever.*

In fact, the temporal dependence of the change in the deformed cantilever shape as a function of the set normal load is clearly illustrated with the SEM micrographs of the grooves shown in Figure 18. It is interesting to notice from these SEM observations that this change is accompanied by a drastic modification of the topography of the groove. This is an interesting phenomenon as it happens in spite of the fact that the force-controlled feedback loop was employed to maintain the A-B voltage constant around a mean value set by the user. In addition, AFM measurements indicate that the grooves became just over 50% deeper and wider on average following such shape transition in the deformed cantilever. This difference in the groove topography is also illustrated in Figure 19 when machining with a set normal load of 34 µN.

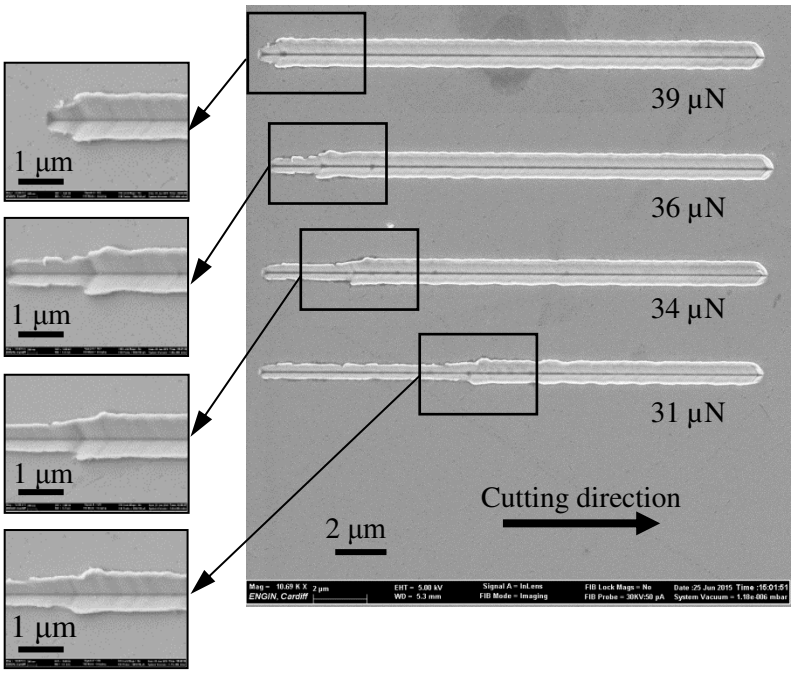

Figure 18. *SEM micrographs of the grooves obtained on the Cu sample when machining in the forward direction with the higher range of set normal loads considered. Scale bar: 4 µm.*

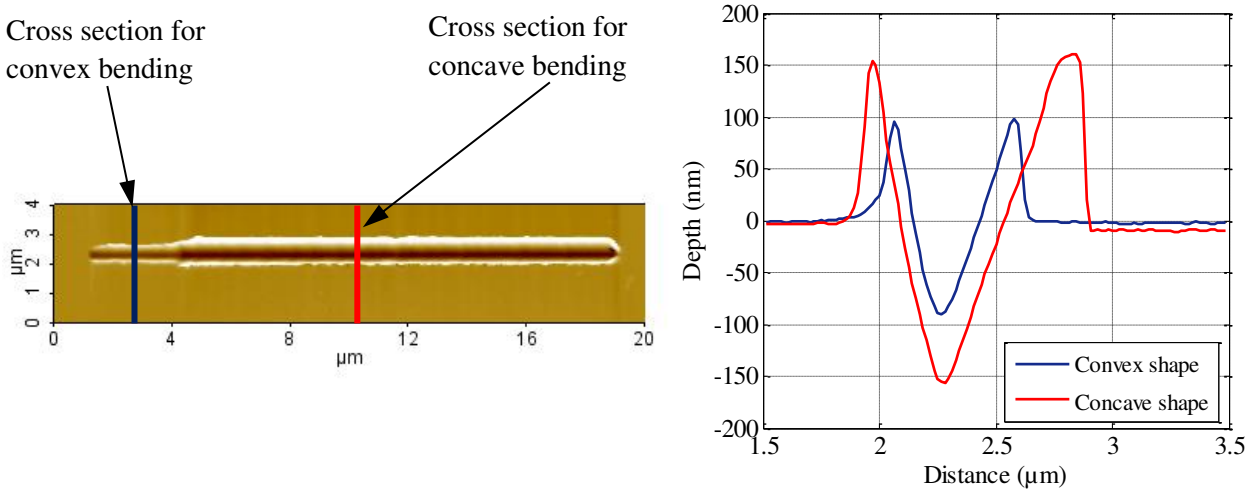

Figure 19. *AFM scan of the groove obtained for a set normal load of 34 µN in the forward direction accompanied with a plot of the considered cross sections.*

In the following section, a confirmation experiment was carried out on the PC specimen to demonstrate that this change in the cantilever shape may also happen when processing along an inclined forward direction or when machining a different substrate or with a different type of probe.

4.3. Verification experiment

In this final experimental run, the PC sample was machined along an inclined angle of 22.5˚ with respect to the pure forward direction (see Figure 4). The set normal forces applied were comprised between 3.1 µN and 4.4 µN. The probe employed was the TESPD type. Until 4.1 µN, the recorded data for the Z-detector signal indicated that the bending of the cantilever kept a convex orientation throughout. As an example, the data obtained with a load of 3.1 µN are given with Figure 20a. However, when the load was raised to 4.4 µN, a rapid increase in the Z-detector signal was recorded during the cutting of the groove as reported with Figure 20b. In this case, the transition from convex to concave bending took place at the start of the groove. Thus, while the occurrence of the cantilever shape modification could be confirmed using a different set of experimental conditions compared to those reported in the previous section, it is interesting to note that, the

transition from convex to concave bending was very sensitive to a small increment in the set normal load applied.

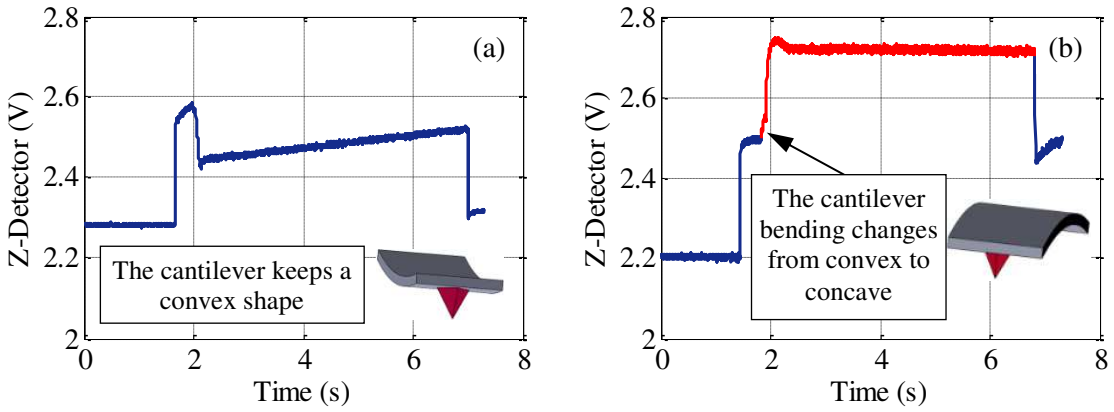

Figure 20. *Recorded Z-detector signals obtained when machining the PC specimen along the inclined forward direction for a set normal applied load of (a) 3.1 μN and (b) 4.4 μN.*

5. Conclusions

This paper describes an important phenomenon specific for AFM nanomachining in the forward direction: under certain processing conditions, the deformed shape of the cantilever probe may change from a convex to a concave orientation. It is argued that the assumption commonly adopted in the literature that the deformed shape of the AFM cantilever used for tip-based nanomachining along the forward cutting direction, is always concave, is wrong. To explain and justify this claim, a refined theoretical analysis of the work of an actual AFM probe is performed, along with the introduction of a new experimental set-up for the determination of the actual cantilever deflected shape during AFM nanomachining. Based on the theoretical analysis, it is shown that the bending of the cantilever during nanomachining in this direction can be convex, especially for small value of the cutting force acting on the tip in the direction of cutting F_a relative to the force needed to keep the tip in the workpiece F_t.

The experimental evidence provided that both (concave and convex) bending orientations of the cantilever could be observed during actual machining tests. These results are based on the combined analyses of three different output signals monitored during processing in addition to the subsequent inspection of the machined topography by producing grooves.

The results provided from both theoretical analysis and experimental work can add other interesting outcomes. Firstly, this study indicates that the analysis of the Z-detector signal is relatively rich and provides valuable data for understanding the mechanical behaviour of the cantilever deflected shape. Secondly, this research suggests that following the initial vertical engagement of the tip into the substrate material, the tip may subsequently slide upwards on the face of the created indent when the lateral motion of the AFM stage begins. This observation was made for the small values of set normal loads considered. For increased values, the tip was more likely to stick onto the face of the indent at this specific stage of the process. Thirdly, the analysis of the Z-detector voltage suggests that AFM nanomachining is achieved in a minimum of five steps, namely, approach, indentation, transition, scratching and reset step. This analysis may be used to gain an improved understanding of the hardware and physical considerations of AFM.

Finally, this study provides an evidence that not only the applied load has an effect on the depth and width of the groove, but also the deflected shape of the AFM cantilever has a significant influence on the trench shape. The latter phenomenon may cause that the trench becomes deeper and larger. For example, it has been observed that the groove becomes over 50% deeper and wider on an average when the cantilever deflected shape changes from convex to concave.

Thus, this research highlights the importance of considering the non-rigid nature of AFM probes when studying the AFM tip-based nanomachining process.

Acknowledgements
The reported research was partially funded by the Engineering and Physical Sciences Research Council (EPSRC) under the grant EP/M020703/1. Raheem Al-Musawi would also like to thank the Iraqi Ministry of Higher Education and Scientific Research (MOHESR) and Kufa University, Department of Mechanical Engineering in Iraq for the financial support provided. F.M. Borodich has been involved in the studies within the CARBTRIB International Network; he is grateful to the Leverhulme Trust for financial support of network. All data created during this research are openly available from Cardiff University data archive at *http://dx.doi.org/10.17035/d.2016.0009233131*.

References

[1] Tseng A A 2011 Removing material using atomic force microscopy with single-and multiple-tip sources *Small* **7**(24) 3409-3427
[2] Yan Y, Geng Y and Hu Z 2015 Recent advances in AFM tip-based nanomechanical machining *International Journal of Machine Tools and Manufacture* **99** 1-18
[3] Tseng A A, Notargiacomo A and Chen T P 2005 Nanofabrication by scanning probe microscope lithography: A review *Journal of Vacuum Science & Technology B* **23**(3) 877-894
[4] Engstrom D, Porter B, Pacios M and Bhaskaran H 2014 Additive nanomanufacturing - A review *Journal of Materials Research* **29** 1792-1816
[5] Dimov S, Brousseau E, Minev R and Bigot S 2012 Micro- and nano-manufacturing: Challenges and opportunities *Proceedings of the Institution of Mechanical Engineers, Part C: Journal of Mechanical Engineering Science* **226** 3-15
[6] Xie X N, Chung H J, Sow C H and Wee A T S 2006 Nanoscale materials patterning and engineering by atomic force microscopy nanolithography *Materials Science and Engineering: R: Reports* **54**(1) 1-48
[7] Tseng A A, Kuo C F J, Jou S, Nishimura S and Shirakashi J I 2011 Scratch direction and threshold force in nanoscale scratching using atomic force microscopes *Applied Surface Science* **257**(22) 9243-9250
[8] Ruan J A and Bhushan B 1994 Atomic-scale friction measurements using friction force microscopy: part I - general principles and new measurement techniques *Journal of Tribology* **116**(2) 378-388
[9] Malekian M, Park S S, Strathearn D, Mostofa M G and Jun M B G 2010. Atomic force microscope probe-based nanometric scribing *Journal of Micromechanics and Microengineering* **20**(11) 115016
[10] Hassani S S and Aghabozorg H R 2011 Nanolithography study using scanning probe microscope. In: Recent Advances in Nanofabrication Techniques and Applications, editor: Cui B. InTech, Rijeka, Croatia
[11] Geng Y, Yan Y, Xing Y, Zhang Q, Zhao X and Hu Z 2013 Effect of cantilever deformation and tip-sample contact area on AFM nanoscratching *Journal of Vacuum Science & Technology B* **31**(6) 061802
[12] Geng Y, Zhao X, Yan Y and Hu Z 2014 An AFM-based methodology for measuring axial and radial error motions of spindles *Measurement Science and Technology* **25**(5) 055007
[13] Timoshenko S. 1940, Strength of materials. Part 1. Elementary theory and problems. Van Nostrand Company, New York, USA
[14] Varenberg M, Etsion I and Halperin G 2003 An improved wedge calibration method for lateral force in atomic force microscopy *Review of Scientific Instruments* **74**(7) 3362-3367
[15] Asay D B and Kim S H 2006 Direct force balance method for atomic force microscopy lateral force calibration *Review of Scientific Instruments* **77**(4) 043903
[16] Merchant M E 1945 Mechanics of the metal cutting process. I. Orthogonal cutting and a type 2 chip *Journal of Applied Physics* **16**(5) 267-275
[17] Manjunathaiah J and Endres W J 2000 A new model and analysis of orthogonal machining with an edge-radiused tool *Journal of Manufacturing Science and Engineering* **122**(3) 384-390
[18] Megson T H G 1987 Strength of materials for civil engineers. Second edition, Edward Arnold (a division of Hodder and Stoughton Ltd), Sevenoaks, United Kingdom
[19] Quintanilla M A S 2013 Surface analysis using contact mode AFM. In: Encyclopedia of Tribology, editors: Wang, Q.J. and Chung Y-W., Springer Science+Business Media, New York, USA.
[20] Sader J E, Chon J W and Mulvaney P 1999 Calibration of rectangular atomic force microscope cantilevers *Review of Scientific Instruments* **70**(10) 3967-3969